Topological Structure and Nonaffine Swelling of Bimodal Polymer Networks

Jens-Uwe Sommer* and Stefan Lay†

Institut de Chemie des Surfaces et Interfaces et Université Haute Alsace, 15, rue Jean Starcky, F-68057 Mulhouse Cedex, France

Received April 8, 2002

ABSTRACT: Using the bond-fluctuation model, we study bimodal networks obtained from end-linking long (100 repeat units) and short (5 repeat units) chains in the melt state. The short chains are dilute among the long chains but provide the majority of chain ends. We discuss the necessary conditions under under which the end-linking process results in the formation of clusters of short chains within the network structure. In our simulations, the onset of this behavior can be observed. On the other hand, the tendency of short chains to form loops is much increased. In the melt state, these loops are likely to form trapped-entanglement long chains, thus yielding a very particular topological structure. We swell the cross-linked systems in an athermal solvent close to equilibrium. The swelling process can be subdivided into two steps. A fast intrusion of solvent into the network provides a large part of the swelling ratio. This is followed by a slow relaxation process, which allows for cooperative reorganization of the network. Our simulations show that swelling of individual strands is highly subaffine. Unfolding of the network structure is necessary in order to provide the global swelling ratio. We systematically analyze the dependency of nonaffine deformation processes as a function of the size of connected substructures. As a result, we conclude that clusters comprising hundreds of strands are necessary to provide affine behavior. These findings can be related to the topological structure formed by the cross-linking process. In particular, we define a folding length which corresponds to the minimal topological distance along the network structure which connect two neighboring monomers in space. The distribution of folding lengths shows a broad peak in the range of the observed nonaffine swelling behavior. Our results show that entanglement constraints do not suppress unfolding of the network structure and challenge simplified theoretical models.

1. Introduction

Polymer networks represent a particular class of materials dominated by frozen-in disorder. During the cross-linking process, new chemical bonds are formed randomly between monomers of interpenetrating linear chains. In marked contrast to the gelation of small molecules, even far above the gel point (which is usually very low for long polymers), the connectivity between monomers is related to the random conformations of the precursor polymers at the moment of cross-linking. This random connectivity, denoted as network topology, is invariant (and thus frozen-in) for all possible conformations of the network and determines the thermodynamic properties, in particular the elasticity, of a rubber. The aspect of the full many-body problem of polymer networks has been emphasized already in the framework of the Gaussian network model (so-called phantom model) introduced by James and Guth; see ref 1. Here, the random connectivity between the monomers can be mapped into a stochastic matrix describing the Gaussian correlations between the monomers.[2] Unfortunately, an explicit solution of this problem is largely restricted to numerical methods.[3,4] Moreover, aspects concerning the swelling behavior of polymer networks cannot be easily implemented into a Gaussian model.

Since the network topology is not accessible directly in experiments, its nature and impact on material properties remained a subject of controversial discussions. One of the open questions is the role of individual network stands and the degree of *affinity* which one can assume for them under external deformations.[5] It was suggested repeatedly in the context of swelling experiments that unfolding mechanisms of the network structure during swelling should play an important role.[6−8] This assumption, however, is in contrast to the prediction of elaborated mean-field-based approaches.[9−11]

Now, large scale computer simulations can shed more light on this yet unresolved problem. Only for simulated systems can one explore the network topology in all details and follow the positions of each repeat unit under external deformations.[4,12−19] However, as our results will also demonstrate, only large scale simulations carried out over a very long simulational time can provide reliable results about the equilibrium state of polymer networks in the dry as well as in the swollen state.

In previous work,[13,15,20−22] we have already investigated the network topology of different types of networks. As a common result of all these studies, we found that clusters of many network strands which are strongly interpenetrated (folded into each other) play an important role for the swelling and segregation behavior. The decomposition of the network structure into chain clusters, where the clusters are connected among each other to form a homogeneous structure, introduces some heterogeneity in the network topology. In fact, following the path of connected monomers in network structures, we usually reach the size of the simulation box before a true three-dimensional behavior of the network structure could be found.[13,20,21]

However, this heterogeneity has a delicate aspect being a heterogeneity of the internal structure. In the

* To whom correspondence should be addressed.
† Present address: FJA Innosoft GmbH, Sachsenring 83, 50677 Köln, Germany.

10.1021/ma0205515 CCC: $22.00
Published on Web 11/14/2002

dry state, the network is spatial homogeneous. The aspects of topological heterogeneity come into play for swelling experiments where depending on the preparation conditions, the topological heterogeneity expands into a spatial heterogeneous structure.[23] Also strong segregation forces as observed in cross-linked blends or interpenetrating networks can bring this heterogeneity to our attention.[22] On the other hand, stretching experiments in the dry state can a priori not display the heterogeneous topological structure directly. In this case, the dynamics related to structural heterogeneities such as the cooperative rearrangement of large parts of the network structure should be considered. In fact, the unusual long-time relaxation behavior of polymer networks under uniaxial stretching has been discussed very early and has not been resolved yet.[24−30]

Here, we present the results of large-scale Monte Carlo simulations using the bond-fluctuation model (BFM) applied to bimodal polymer networks. This special class of end-linked networks received some attention for their particular material properties. On the other hand they can serve as the simplest and well-controlled realization of a strong polydispersity effect as it occurs naturally in randomly cross-linked networks.[21,31] Some open questions concerning the structural properties of these systems, such as the "clustering problem" of small chains can be addressed in our simulations as well. We have calculated the statistics of folding lengths, which we have introduced in a previous letter,[32] and investigated the unfolding process of connected clusters of network strands in great detail during athermal swelling.

The rest of this work is organized as follows: In section 2, we review the model of a folded network topology taking the point of view of the "internal geometry". In section 3, we briefly discuss the simulation model and the preparation of bimodal networks. The topological properties, in particular the distribution of folding lengths are discussed in section 4. The swelling behavior of our network structures is investigated by following connected substructures of the network as well as the individual network strands during swelling in section 5. We discuss our results in section 6.

2. Cross-Link Topology and Folded Network Structure

Cross-linking dense, interpenetrating chains results in a structure where the linear connectivity of the precursor polymers still plays an important role. Unlike percolation of small molecules, most of the spatial neighbors of a given cross-link within the range of a "bond" (which is a strand in this case) are not directly connected to this cross-link. Let as consider the simplest case of chains consisting of N statistical repeat units which are perfectly cross-linked at their chain ends. Unter melt conditions (screened excluded volume) these chains display a Gaussian conformation statistics. Therfore, $n_F \sim N^{1/2}$ other chains reside in the volume of gyration of a given chain. Only f (functionality of cross-links) out of these n_F chains will be actually attached to the given chain and will become its direct topological neighbors. This situation is illustrated in Figure 1. If we would start from a given monomer and follow the inner, topological structure, we would visit regions far from the origin before we would come back to visit part of the immediate spatial neighborhood of the starting point. Therfore, in the dense state, the network structure must be folded similar to a crumpled up sheet of paper. As a consequence, we have to distinguish between inner topological properties and outer conformational properties of the network structure.

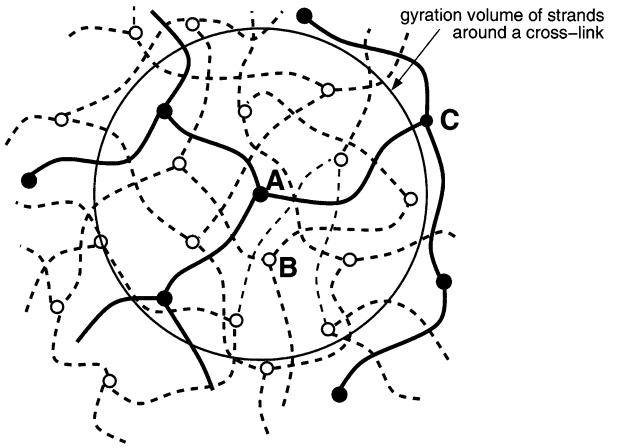

Figure 1. Illustration of the relation between topological and spatial neighbors. If we pick out a cross-link and consider the first generation of topological neighbors (filled circles) we find many chains and cross-links which must not belong to this topological neighborhood because individual strands do by far not fill space densely. A given cross-link **A** has therefore much more spatial neighbors **B** then direct topological neighbors **C**. If the network is perfectly connected (no sole part) also these type-**B** cross-links must have a topological connection to **A**. As a results the topological structure must be mapped in a folded way into the three-dimensional space.

The most important question is now, *to what extend this folded structure can be unfolded or rearranged* under external deformations or during diffusion dynamics of the monomers. In other words: Does this nontrivial network topology has an impact on the network entropy? If the cross-links would be the only restriction for the chains (phantom model),[1] unfolding could take place to a maximal extent and would be an important feature of such a system.[5] Then, we must ask for a characteristic size L above which homogeneous deformations take place. Let us call a substructure of this size a *leaf* and consider the network as a superstructure made of connected leaves. In swelling experiments such leaves unfold and disentangle to a certain amount which gives rise to spatial heterogeneities on scales much larger that the averaged strand length. On the other hand, for uniaxial dry deformations, relaxation times for approaching stress−strain equilibrium are determined by the refolding dynamics of leaves.

Frequently, the idea has been put forward that the presence of trapped entanglements between the network strands suppresses such an unfolding processes widely, see ref 5, resulting in nearly affine behavior of cross-links in respect to external deformations. If it is assumed that entanglements restrict the fluctuations of the cross-links,[5] the latter can be thought to be fixed in an elastic matrix which truly follows the external deformations.[33,34] This affine deformation model being an extreme case for the description of network elasticity. However, it is not clear why entanglements will restrict the fluctuations of cross-links and not those of all other monomers as well. Therefore, the tube model for entangled network chains has been introduced.[9,35] A further advantage of the latter is that it can be employed in a self-consistent mean-field approach for the network entropy;[9] see also refs 10 and 11.

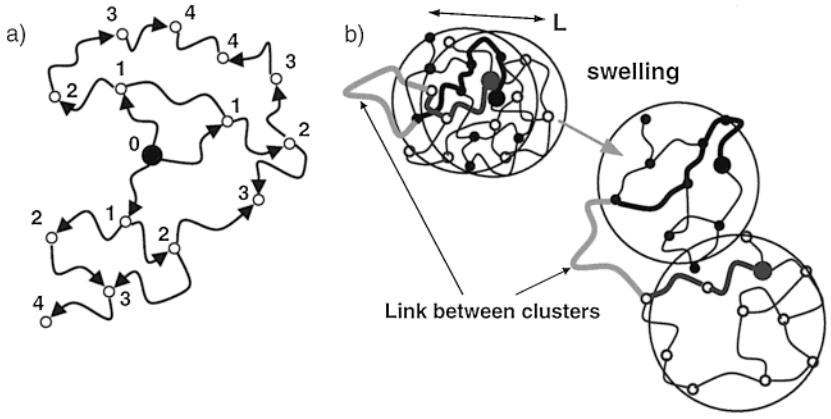

Figure 2. (a) Topological extension of a monomer (filled circle) forming a leave of connected monomers. For simplicity, the order of the topological extension is denoted by numbers counting the cross-links only. (b) Two interpenetrating leaves formed by the topological extension of neighboring cross-links (emphasized by larger symbols). Above a characteristic length scale L (indicated as circumferences) the leaves are connected thus realizing a topological path between the two neighboring cross-links (indicated by thicker lines). During swelling, leaves start to deinterpenetrate first (unfolding) and individual stands are deformed only weakly.

However, if we reconsider our arguments about the network topology (that is taking the point of view of the "internal geometry"), these models have to be contested. The basic hypothesis in the classical approach to the entanglement problem is that *homogeneity is assumed a priori*, either directly[5] or indirectly, by applying a mean-field solution.[9] By contrast, one can show that entanglements do not change our conclusions about the folded network structure qualitatively but only in a quantitative way. Let us consider trapped entanglements (only these can be relevant for equilibrium statistics) localized as *slip-links*, that is additional cross-links which can slide along the connected chains. Then, the simplest way to take into account the effect of entanglements is to replace them by additional effective cross-links by fixing their positions along the connecting chains. Since the additional freedom of slip-links makes them less efficient in restricting the chain conformations compared to chemically fixed cross-links,[36] we overestimate the action of entanglements by counting them as additional cross-links.

As a result, we just have to introduce an effective strand length $N_{\mathrm{eff}} < N$, and all the arguments given above must apply to the generalized or effective cross-link topology. Thus, the picture of localized, trapped entanglement does not give rise automatically to an homogeneous network structure. Of course, the resulting effective strand length N_{eff} has to be still large enough to allow for the discrepancy between topological and spatial neighbors, which gives rise to the folded network structure. Now, the contribution of trapped entanglements can be estimated form the elastic modulus of polymer networks as a function of the cross-link density. As a result, the typical entanglement contribution is rather low (about one-third of the total modulus for very lightly cross-linked systems).[27] Compared to real systems, the cross-link density in our simulations is very high (about 20 statistical monomers between cross-links) meaning that the *contribution of entanglements to the effective cross-link density* (and the effective strand length) is rather low.

On the other hand, an amount of trapped entanglements which reduces the size of effective strands to such small values so that n_{F} goes to zero would unavoidably lead to an extraordinary high elastic modulus of the network which is not observed. Therefore, we can draw the following general conclusion: *The experimental fact of a low elastic modulus together with the Gaussian properties of (effective) network strands leads to the ultimate conclusion of a folded network structure.* Since the entanglement constraints are taken into account, no additional homogenizing effect can be assumed which prevents a priori a possible unfolding process under external constraints. However, the effect of the entanglements can be very important in determining the leaf size of the folded structure.

Let us proceed to find an appropriate measure to analyze the network topology and its impact on the statistics of networks. We do so by defining the topological neighborhood of generation g of a given monomer A which we call the *topological extension* $\mathcal{T}_g$(A). This idea is sketched in Figure 2a. In the first step we search for all monomers which are directly connected to A. This forms the first generation $\mathcal{T}_1$(A) of the topological extension of A. In the second step, we search for all monomers which are directly connected to each of the first generation of monomers and are not counted before. Together with the already counted monomers this gives $\mathcal{T}_2$(A). If we proceed successively for g steps we obtain a connected structure of $M(g)$ monomers which corresponds to all monomers which can be reached within g steps along the network topology. Thus, the topological extension is a possibility to define a sphere on an arbitrary topology. Let us now define an inner or chemical dimension d_{i} of a so obtained substructure in the following way:

$$M(g) \sim g^{d_{\mathrm{i}}} \tag{1}$$

For large values of g we expect a three-dimensional behavior of the network structure, that is $d_{\mathrm{i}} = 3$. For regular lattices such as a diamond structure, this limit would be achieved after only a few generations of cross-links have been passed.

Using this concept, we can define a topological distance D(A,B) between two monomers A and B as the shortest path which connects two monomers along the network topology. Since the difference between spatial and topological neighbors is the essential argument for the folded network structure, the topological distance

between two spatial neighboring monomers should be most characteristic for the folded structure. Therefore, we define a *folding length D* as

$$D = D(|\mathbf{r}_A - \mathbf{r}_B| \leq r) \tag{2}$$

where r defines the range of the spatial neighborhood. An alternative way to define the folding length is to consider the topological extensions $\mathcal{T}_{g1}(A)$ and $\mathcal{T}_{g2}(B)$ for two neighboring monomers A and B having a spatial distance not larger than r. The folding length is then given by the smallest value $g = g_1 + g_2$ where both topological extensions have a common monomer. The characteristic extension in space which is reached during this process for each leave is denoted by L. This idea is sketched in Figure 2b.

3. Preparation of Bimodal Networks and Segregation of Small Chains

We use the bond-fluctuation model (BFM) on a three dimensional cubic lattice. Details of this model are given elsewhere.[37] The basic idea is as follows: One repeat unit occupies a elementary cell of a cubic lattice, that is eight lattice sites. No overlap between repeat units is allowed (excluded volume conditions). Bonds between repeat units are restricted to a given set of vectors which is chosen to prevent any chain crossing events during elementary steps (in our case this corresponds to a move of a single repeat unit by only one lattice unit (LU) in one of the six possible directions of the cubic lattice). Therefore, cut-avoiding (conservation of trapped entanglements) is realized within this model under the condition of excluded volume. The length of bonds can vary in a range between 2 and $\sqrt{10}$ LU. Because of the bond restriction, the lattice occupation is effectively increased. A lattice occupation of about $\rho = 0.5$ corresponds to the behavior of a highly concentrated system and reflects the state of polymer melt.[38] Additional free volume corresponds to athermal solvent. Random local moves result in a realistic diffusion dynamics on scales larger than the lattice unit.

The network is prepared in three steps. We start by equilibrating a melt of $M_L = 5000$ chains of length $N = 100$ in a simulation box having the extension of $200 \times 200 \times 200$ LU (occupation density of $\rho = 0.5$). Then, part of the melt chains are cut in smaller chains of length $P = 5$, followed by an equilibration run. In a third step, the equilibrated bimodal melt is cross-linked by adding a stoichiometric fraction of 12 504 cross-linkers of functionality $f = 4$ to the systems (thus increasing the lattice occupation density to $\rho = 0.5125$). The cross-linkers are attached directly to randomly chosen chain ends. Now, the usual MC-dynamics consisting of single moves is applied. The cross-linking process is modeled as a result of a collision process between functionalized monomers (chain ends and cross-linkers). If a collision between a cross-linker and a free chain end would have taken place (the step is rejected then because of excluded volume), a new bond is formed instead if the cross-linker is not already bound to four chain ends. We have stopped the cross-linking process after 600 000 Monte Carlo steps (MCS) which results in a network with a gel fraction of 0.9854 (largest connected cluster). The most relevant parameters are summarized in Table 1.

The most interesting effects have been observed experimentally for bimodal networks when the short chains are dilute among the long chains (most of the monomers belong to long chains) but provide the majority of chain ends (most of the cross-links belong to short chains).[39] This can only be realized by a large ratio Γ between the chain lengths

$$\Gamma = N/P \gg 1 \tag{3}$$

For a small volume fraction of short chains $c \ll 1$, we obtain for the molar fraction p of short chains

$$p = \frac{c\Gamma}{1 + c\Gamma} \tag{4}$$

Consider a value of c which is small enough that the short chains do not overlap in the melt state, that is $c \ll c^*$. The overlap concentration c^* is now related to the chain length by

$$c^* \sim P^{-1/2} \tag{5}$$

Here, the short chains adopt a Gaussian conformation statistics (long chains screen their excluded volume interactions). Now, we assume that Γ is large enough to ensure that $1 - p \ll 1$. In this case, the ends of long chains are highly diluted, and almost all reactive chain ends belong to the small chains. Hence, the short chains will react under dilute conditions while the long chains are forming a quasinonreactive background. This situation is sketched on the left-hand side of Figure 3.

Because in the cross-linked state the strands have to be as close as their radius of gyration, the concentration must locally increase to c^*, under dilution of other parts of the volume. Thus, a density instability occurs which leads to an increase of concentration fluctuations followed by a tendency toward segregation of short chains. Since cross-linking is a highly irreversible process (the activated melt is very far from the chemical equilibrium), the resulting structure is kinetically controlled and results in the formation of cluster of connected short chains. Since the diffusion coefficient of these clusters decreases inversely proportional to their mass, coalescing processes between clusters are unlikely, if the reaction rate is high enough. Compared to this growth processes the nucleation of new clusters is relatively improbable due to the low concentration. (The rate of nucleation of two chain is proportional to c^2.) Thus, a structure is build up by growing clusters where from time to time a single chain end of a long chain is incorporated. On the other hand, these trapped long chains form long-range connections between short-chain clusters, thus producing a connected superstructure of

Table 1. Properties of the Simulated Networks

property	value
lattice	$200 \times 200 \times 200$, cubic
boundaries	reflecting (solid walls)
lattice occupation	0.5 melt, 0.5125 cross-linked
short chains	$P = 5$, $n_P = 21060$
long chains	$N = 100$, $n_N = 3947$
av strand length	$\langle N \rangle = 20$
vol fraction (short chains)	$c = 0.21$
mol fraction (short chains)	$p = 0.84$
no. of cross-links	$n_C = 12504$
functionality	$f = 4$, $\langle f \rangle = 3.9$
gel fraction	$c_{gel} = 0.985$

[a] We use the following notation: P, length of short chains; N, length of long chains; $\langle N \rangle$, average strand length; n_X, number of X chains; c, volume fraction of short chains; p, mole fraction of short chains, f, functionality of cross-links; c_{gel}, gel fraction.

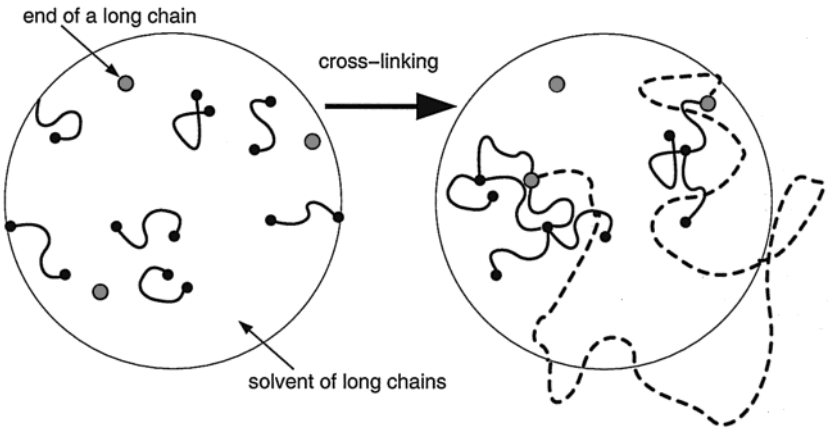

Figure 3. Cross-linking process in the limit of diluted short chains. If the volume fraction of short chain is much below the overlap threshold it is still possible that the overwhelming part of the chain ends, that is the reactive groups, belong to the short chains. The cross-linking reaction will force a local increase of the concentration of short chains and therefore the formation of clusters of short chains which are connected by strands of long chains.

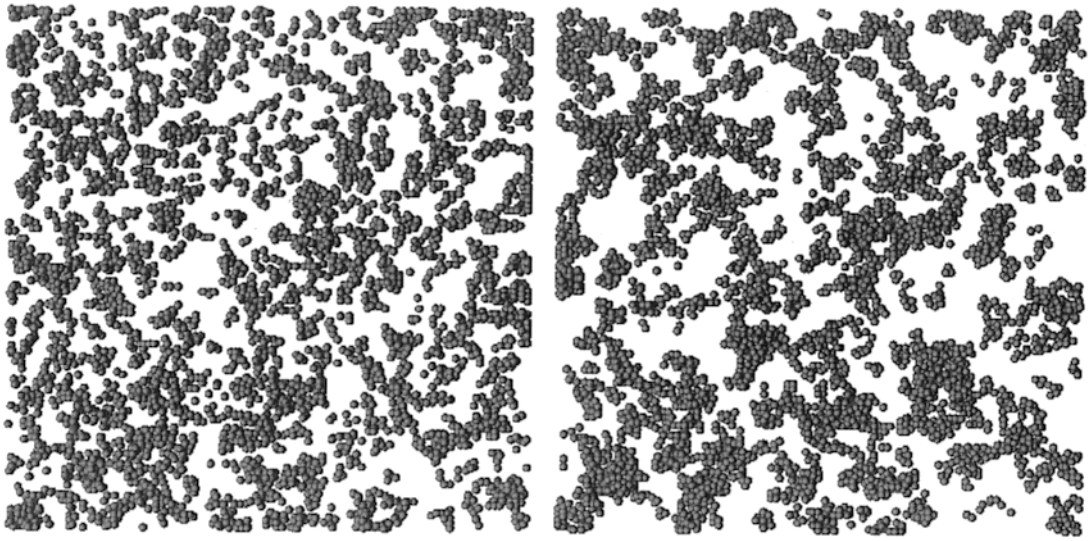

Figure 4. Snapshots of configurations of short chains within a thin slice (10 LU) before (left) and after cross-linking (right). The end-to-end distance of the short chains is about 6 LU.

the final network. This situation is illustrated in the right-hand side of Figure 3. Also, the short chains can form an infinite cluster (subnetwork) if c is not too low. Such a process would result in huge fluctuations of the short chain density, resulting in significant results for scattering experiments on appropriately labeled systems.[40]

On the other hand, if c is larger than c^*, segregation of short chains will not take place. In the semidilute regime the mean separation between chain ends is less than the averaged radius of a precursor chain. Thus, the precursor chains find sufficient reaction places in the immediate neighborhood and the density of the short chains can be maintained during the cross-linking process. Since the molar fraction of short chains should be close to unity ($p \simeq 1$), we can estimate the crossover condition for short chain clustering using eqs 4 and 5 in terms of Γ as

$$c^*\Gamma \gg 1 \tag{6}$$

This yields to the following relation between short and long chains which must be fulfilled for clustering

$$P \ll N^{2/3} \tag{7}$$

Since numerical prefactors cannot be obtained from this scaling analysis, the inequality should be limited to the strong case. Although this inequality is satisfied for the simulated network, it should be considered already as a limiting case as the following analysis shows.

In our simulations, the relative volume fraction of the short chains is $c = 0.21$ which corresponds to a lattice occupation of 0.1053. In Figure 4, cuts through the central part of the simulation box are displayed which visualize only short chains. The thickness of the slice is taken to be close to the correlation length of the cluster structure in the cross-linked system, being of the order of 10 LU, see below. The enhancement of concentration fluctuations due to cross-linking can be clearly observed, although the effect is not dramatic since the volume fraction of short chains is still close to c^*. Moreover, the short chains form a percolating cluster *within* the connected cluster of all chains. The percolation threshold of short chains is reached after about 15 000 Monte Carlo steps during the cross-linking process. At this point the effective cross-link functionality is given by $f_{\text{eff}} = 3.575$, while at the final stage we have $f_{\text{eff}} = 3.901$, see Table 1. Therefore, the *short chains form a well-connected subnetwork* within the overall network structure. This will be of importance

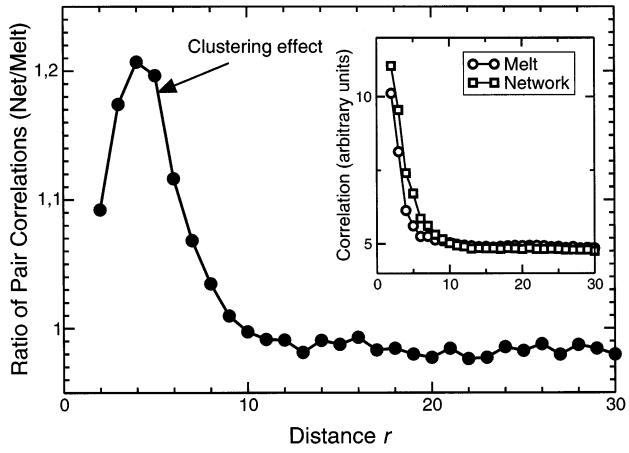

Figure 5. Ratio of the radial pair correlation functions between the network and the un-cross-linked melt. The individual correlation functions are display in the inset. Here, we calculated the volume fraction of short chains within a shell of thickness of 1 LU at distance r from the origin (which is a repeat unit of a short chain). Averaging has been obtained by considering all repeat units of short within a box of 80 × 80 × 80 LU in the center of the simulation box as origin for the calculation.

for the discussion of the nonaffine swelling behavior in section 5.

A more quantitative analysis is given in Figure 5. Here we display the ratio of the pair correlation functions of short chains in the cross-linked state and the melt state, respectively. We have calculated the pair correlation function directly as the volume fraction of short chains in a 1 LU thick shell of radius r around the origin formed by a repeat unit of a short chain. The increase of concentration fluctuations of short chains due to cross-linking can be clearly seen from the pronounced peak between 3 and 10 LU.

To conclude this part, we have found evidence for the increase of concentration fluctuations of short chain due to cross-linking. A larger ratio Γ, together with a smaller volume fraction of short chains is necessary to observe a more pronounced segregation effect of small chains during cross-linking.

Another interesting property of bimodal networks is the high probability of forming loops of short chains using two functionalities of the cross-linker. The fact that short chains have to travel relatively long distances until a reaction with an end group of a different chain can take place, increases this probability further. Under the conditions of our simulations already 27% of the short chains form self-loops (for comparison, only 0.6% of long chains form self-loops), although the contribution of the dilution effect during cross-linking is not dominant here. However, this has an interesting consequence for the topological structure: Since the short chains are diluted among long chains without solvent, these loops are likely to enclose strands of long chains. Thus, the loop formation yields a relative increase of the density of trapped entanglements.[41,42] As a result the clusters of short chains can bind many long chains additionally in short-loop slip-links, an effect which is similar to the adsorption of network chains by filler particles. Indeed, the relation between clusters of short chains in bimodal networks and filler particles was anticipated previously.[43]

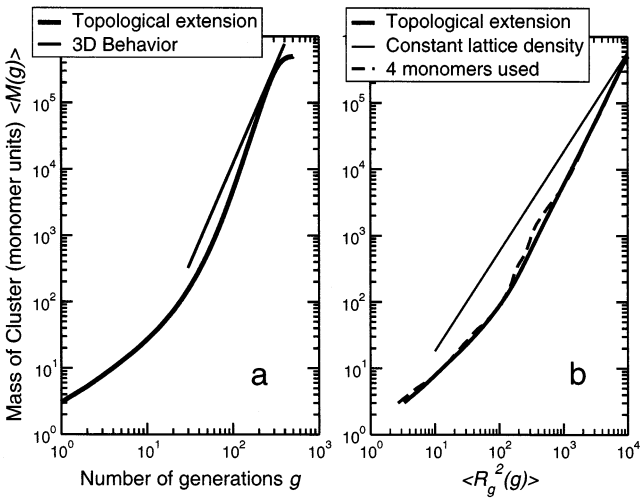

Figure 6. (a) Total mass of the topological extension $M(g)$ as a function of the number of generations g averaged over topological extensions of all monomers within a sub-box of size 30. The straight line corresponds to the limiting three-dimensional behavior. (b) Total mass of the topological extension is plotted against the mean square radius of gyration. For comparison, the corresponding behavior for a homogeneous sphere according to eq 8 is displayed. The dotted line corresponds to the result obtained by averaging only over the topological extension of four monomers.

4. Topological Properties and Folding Length

We are now going to analyze the structure of the obtained network according to the lines given in the section 2. First of all, we search for the largest connected cluster. This cluster contains 504 599 repeat units, which corresponds to a gel fraction of 0.9854 (the second largest cluster contains only 228 repeat units). In most of the following results we restrict ourselves exclusively to the gel fraction. Now, the topological extension is calculated, see Figure 2a, for each monomer (which is part of the largest cluster) within a sub-box of size 30 located in the center of the simulation box. The averaged mass $\langle M(g)\rangle$ obtained in this procedure is plotted in Figure 6a) as a function of g. As for all of our previous simulations,[13,15,20,21] we obtain a behavior which differs significantly from a regular three-dimensional mesh.[21] For $M(g)$ smaller than 100, which corresponds to the mass of the long chains, the apparent internal dimension d_i, see eq 1, is slightly larger than unity, which is caused by branching events which occur with the probability $1/\langle N\rangle$ for a randomly chosen start monomer. This regime is followed by a upturn the function $\langle M(g)\rangle$ with an apparent internal dimension $d_i > 3$. A value of d_i larger than the dimension of the embedding space is possible because the topological extension is not compact up to very large values of g, which allows a more open branching. Only for very large values of $M(g)$ (more than 100 000 repeat units) a three-dimensional behavior is forced. At the same time, border effects come into play. Therefore, it is even possible that the here obtained crossover behavior is due to the finite size effect of the simulation box.

During the calculation of $\mathcal{T}_g(A)$ we can also follow the spatial configuration of the obtained monomer clusters. In Figure 6b, we have plotted the mean square radius of gyration $\langle R_g^2(g)\rangle$ vs the mass $\langle M(g)\rangle$. If the topological extension would belong to a three-dimensional object, the corresponding slope of the double logarithmic rep-

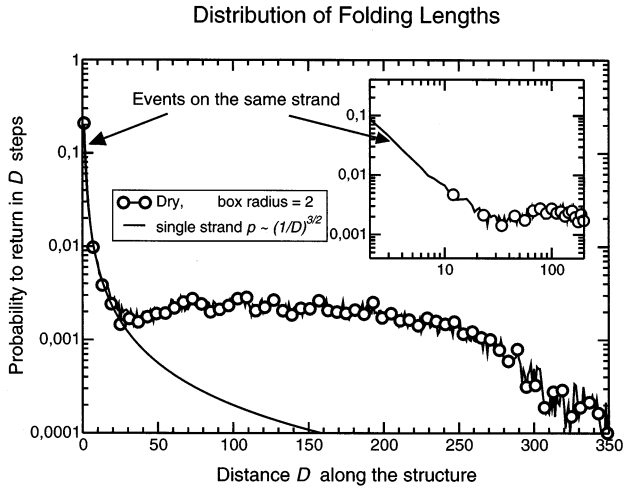

Figure 7. Distribution of folding lengths D for spatial neighbors. The inset shows the double logarithmic representation. Until the size of the average strand length $\langle N \rangle = 20$, return events along the same strand dominate. The expectation of return events along the same chain is indicated by a line in the outer figure.

resentation has to be $^3/_2$. For comparison, we have plotted the behavior of a three-dimensional homogeneous sphere of the average lattice density $\rho = 0.512$. For the number of repeat units in a sphere represented by its radius of gyration one obtains

$$M = \frac{\rho}{8} V = \frac{\rho}{8}\left(\frac{5}{3}\right)^{3/2}\left(\frac{4\pi}{3}\right)(R_g^2)^{3/2} \tag{8}$$

Again, this limiting behavior is only reached for very large structures approaching the size of the simulation box.

In Figure 6b, we have also displayed the behavior averaged over only four start units for the topological extension (core monomers were taken from a $4 \times 4 \times 4$ sub-box only). Compared to the fully averaged function, undulations up to a mass of a few thousand monomers can bee seen. The latter reflect spatial folding of the counted clusters.

Now, let us turn to the distribution of folding lengths introduced at the end of section 2. We start to compute $\mathcal{T}_{g1}$(A) and $\mathcal{T}_{g2}$(B) for two neighboring monomers A and B until a common element is reached. The folding length along the network structure D is then given by the sum of generations reached in each topological extension $D = g_1 + g_2$. Here, we use 10 000 pairs of repeat units located in the center of the simulation box. A repeat unit B is considered to be a spatial neighbor of another repeat unit A, if it is located within a box of size r around A. In Figure 7, the distribution of folding lengths $p(L)$ is displayed for the case $r = 2$ (nearest BFM neighbors on the lattice). For small values of D (smaller than the averaged strand length), there is a relatively high probability for a given repeat unit to find a repeat unit of the same chain as its closest neighbor. This can be easily understood by considering a single bond, that is $D = 1$. The volume of the neighborhood $(1 + 2r)^3$ consists of 125 lattice sites containing in 8 repeat units on average. Excluding the reference unit and assuming that two bonded repeat units are enclosed in the volume, we obtain a probability of $^2/_7 \simeq 0.28$, which reasonably explains the obtained probability of about 0.2. On the other hand, it is obvious that short values of D are most frequently realized by loops formed by single strands.

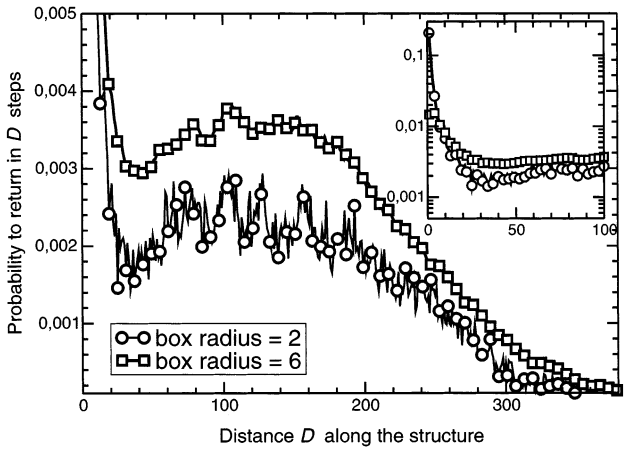

Figure 8. Distribution of folding lengths D with different radius r for counting return events. The inset shows the single logarithmic representation.

Only larger values of D will take into account paths over several cross-links. This overestimation of short loops is corrected if larger values of r are considered. In Figure 8, we compare the distribution of folding lengths shown in Figure 7 with a distribution obtained for $r = 6$ (averaged end-to-end distance of short chains). As expected, the single strand events are less dominating and the distribution of D is extended to even larger values.

As a general property of the distribution of folding lengths, we observe a broad peak centered around $D \simeq 150$ for values of D larger than the average strand length. For $D \simeq 150$, the topological extensions of both start units reach a size of about $R_g \simeq 25$, which corresponds to about 1700 repeat units for each topological extension. Note that the typical extension of such a leaf is much smaller than the box size.

In Figure 9, a snapshot of the conformation of the first 1500 monomers from a topological extension is displayed for monomer A, located in the center of the simulation box. The topological distance g from A is coded in gray scale: White spheres belong to the immediate topological neighborhood of A, while black spheres belong the most distant units measured along the network structure. Although about 75 averaged strands of length 20 are considered, not even the onset of a three-dimensional behavior can be observed. On the other hand we can see already the back-folding of part of the structure (black spheres close to white spheres) as well as the conformational disorder: The crossover from white to black is not reflected as a smooth crossover in the embedding space.

5. Swelling Properties and Nonaffine Deformation

As well-known, polymer networks can take up large amounts of solvent, usually a multiple of their own volume in the dry state. The volume swelling ratio Q is defined as the ratio of the volume of the swollen network V to that of the dry system V_0

$$Q = \frac{V}{V_0} = \lambda^3 \tag{9}$$

Here, λ corresponds to the linear deformation ratio of the swollen sample compared to the dry sample. Using the simple assumption that the swelling consists of

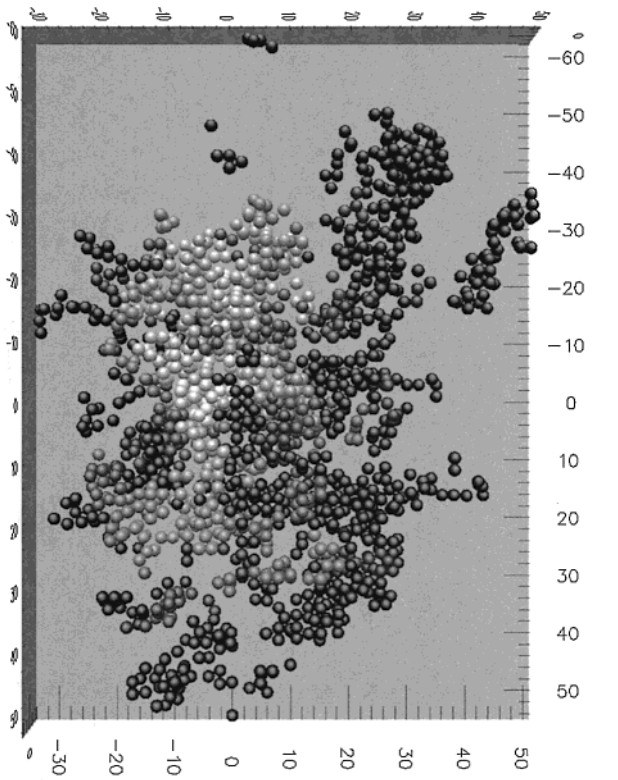

Figure 9. Slice through the conformation of the first 1500 monomers of a topological extension of a repeat unit A located in the center of the simulation box. The topological distance (number of steps to go along the network structure) is coded in gray scales. White spheres belong to the immediate neighborhood of A while black spheres are topologically most apart from A. Seemingly unconnected monomers are due to slicing (slice thickness is 10 LU).

(affine) stretching of individual strands (reduction of elastic free energy), which is compensated for by a gain of entropy due to intrusion of the solvent (mixing free energy, energetic contributions due to solvent−polymer interaction can be included), Flory and Rehner[44] found a simple solution for the swelling degree Q at the equilibrium state. On the other hand, experiments carried out on various systems considering different properties of networks during and after swelling (or deswelling) processes are not in agreement with these simplified assumptions.[6−8,23,45−47] The dispute about the role of a hidden interaction parameter due to cross-linking could not be resolved yet on the basis of experimental work only. Unfortunately, an ideal athermal solvent does not exist, and even very small changes in the interaction parameter can lead to rather large effects within the framework of the Flory−Rehner theory.[6]

Now, for computer simulations, swelling in an ideal athermal solvent is the most simple and direct way to induce a network deformation process. To simulate swelling, the network is put into the center of a larger simulation box. Additional empty lattice places correspond to ideal athermal solvent. For our system, we used a simulation box of size 400 × 400 × 400. In Figure 10, we have plotted the fraction of repeat units per lattice site at a given position z (linear lattice density) for various times of swelling t. After a short time period of less than 50 TMS (thousand Monte Carlo steps), the solvent penetrates the network completely. On the other

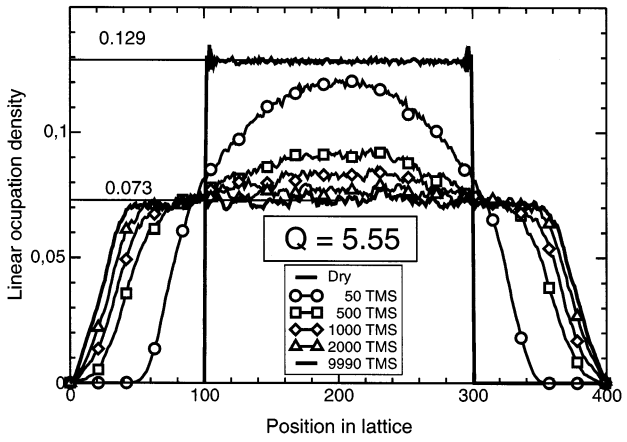

Figure 10. Repeat units per lattice site as a function of one lattice coordinate averaged over all spatial directions. Different curves are obtained for various times that the swelling had started.

hand, about 10 000 TMS are necessary to access a state close to the swelling equilibrium. This shows that diffusion of the solvent molecules is not the rate-limiting process. The slow relaxation processes (about 1000 times the Rouse relaxation time of an averaged stand) must be attributed to cooperative relaxations of larger parts of the network structure. This is most pronounced if we consider the late stages of the swelling process: We need 8000 TMS to obtain a change in the volume swelling ratio from $Q = 5$ to $Q = 5.55$ (compare the curves for $t = 2000$ TMS and $t = 9990$ TMS, respectively). At the same time, the lattice occupation density has reached a value of about 0.1, where moves of the repeat units are very efficient within the framework of the BFM. An obvious question arises: How should an affine deformation process of individual network strands explain the *slow dynamics of network swelling*, in particular close to the equilibrium state?

We are now able to follow the deformation of individual network strands as well as the deformation of arbitrary topological extensions within the network structure. First, we consider the isotropically averaged distribution of the end-to-end distance of the long chains. The latter is given by the average of the distribution of the spatial components for a given distance R, $p_L(R) = {}^1/_3(p_X(R) + p_Y(R) + p_Z(R))$. The second moment of this distribution yields the mean square end-to-end distance per Cartesian component. In calculating the distributions, we exclude a region at the border of the simulation box of thickness 20 and 40 LU for the dry and the swollen state, respectively. The results are displayed in Figure 11 for the un-cross-linked melt, the dry cross-linked system and the network swollen in athermal solvent for 9990 TMS.

Comparing the curves for the system before and after cross-linking shows us no remarkable difference. Also comparing the second moment of the distribution does not give a significant difference beyond the statistical error ($R_{melt}^2 = 331$, $R_{net}^2 = 333$). Therefore, we conclude that the cross-linking process does not change the conformation statistics of the long chains.

We compare now the end-to-end distribution before and after swelling to calculate the degree of swelling for individual long chains. As a guide for the eyes we have added a fitted Gaussian distribution to both curves (which is a rather good approach under the given

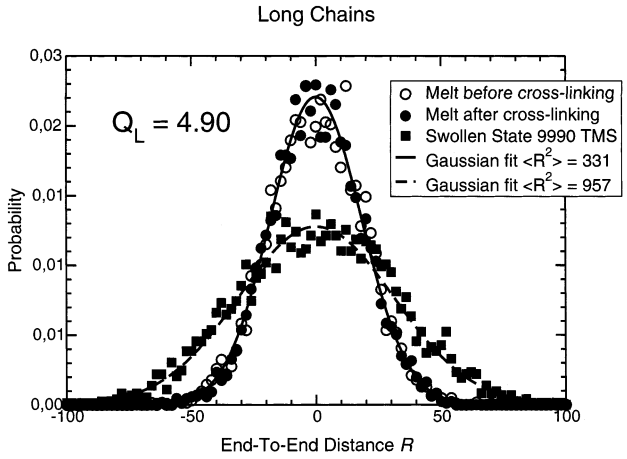

Figure 11. Distribution of the end-to-end distance (per spatial component) of long chains. The effective degree of swelling for the long chains Q_L has been calculated by using the second moments of the distributions.

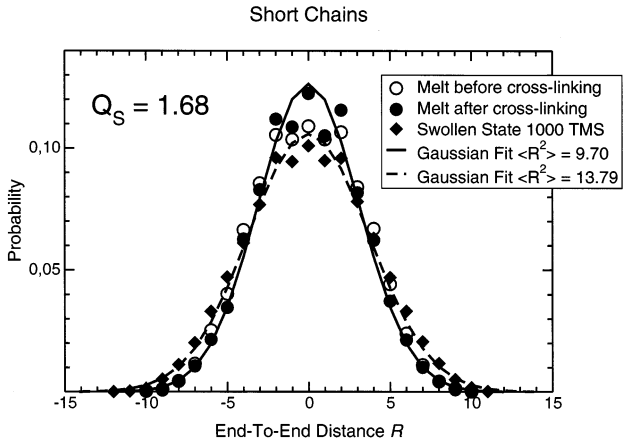

Figure 12. Distribution of the end-to-end distance (per spatial component) of short chains. The effective degree of swelling for the short chains Q_S has been calculated by using the second moments of the distributions.

conditions). We define a volume degree of swelling for the individual long chains as

$$Q_L = \left(\frac{\langle R^2 \rangle}{\langle R_0{}^2 \rangle}\right)^{3/2} \tag{10}$$

where $\langle R_0{}^2 \rangle$ denotes mean square end-to-end distance of the chains in the dry state. This can now be compared to the macroscopic degree of swelling. Our data yield a value of $Q_L = 4.90$, which is below the affine expectation. It is worth noting that even if the long chains would obey the affine condition, this does not mean that the Flory−Rehner theory is valid since the long chain forms only the minority of the elastic active strands in the network.

Let us now turn to the majority of the strands, namely the short chain fraction. The results for the end-to-end distribution are displayed in Figure 12. The local degree of swelling of the short chains differs from the macroscopic value by more than a factor of 3. This observation is very similar to former results obtained for randomly cross-linked systems.[20] The enhanced formation of self-loops can be clearly seen in Figure 12 by comparing the distributions before and after cross-linking around $R = 0$. Note that the short chains form a well-connected

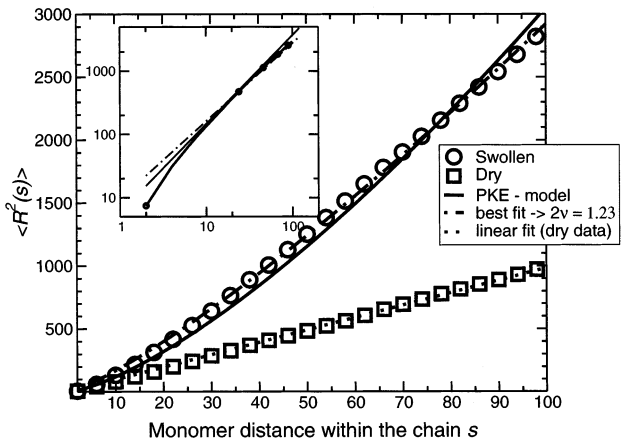

Figure 13. Mean square radius of gyration $\langle R_g{}^2(s) \rangle$ is plotted vs the distance s along the contour of the long chains. In the dry state, a Gaussian behavior is shown, which is indicated by a linear relation $\langle R_g{}^2(s) \rangle \sim s$. For the swollen state, we applied the PKR model with $2\nu = 1.4$. The best fit to the data is obtained with $2\nu = 1.23$. The inset shows the double logarithmic representation of the data in the swollen state.

subnetwork here (see section 3) and not just islands connected by long chains.

Recently, Pütz, Kremer, and Everaers (PKE) have published a model to describe the conformational properties for a single network strand in the swollen state.[48] Using a generalized Flory argument, PKE try to take into account the effect of penetration of n_F chains (see section 2) within the volume of gyration of a given chain. The basic idea is that these chains cannot escape (desinterpenetrate) from their common environment. Instead of the well-known Flory exponent ($\nu = {}^3/_5$) PKE obtain a larger exponent of $\nu_{PKE} = {}^7/_{10}$.[48] According to this idea, we checked the internal conformation statistics for the long chains in our simulations. Starting from the middle of the chain, we calculated the mean square end-to-end distance $R^2(s)$ between monomers having the distance s along the chain's contour. The results are displayed in Figure 13 for the dry and the swollen states, respectively. In the dry state, we expect a self-similar Gaussian behavior which is indicated by a slope of $2\nu = 1$. In the swollen state the PKE-fit is rather moderate. Given the freedom of fitting the ν exponent as well, the best result is obtained for $2\nu = 1.23$. On the other hand, we can make use of our fractal cluster model,[15,32] considering the long chains as shortest paths through the clusters considered as fractal objects with an internal dimension d_i defined in eq 1. This yields $\nu_S = (d_i + 2)/5$. For a value of $d_i = 1.1$, which provides a good fit to simulated[15] as well as to experimental[32] data, we obtain $2\nu_S = 1.24$. This is indeed in rather good agreement with the fitted value. However, a closer analysis and comparison of both models on the basis of various simulated network topologies would go beyond the scope of this paper and will be the subject of future work. Note that also the PKE model involves cooperative behavior of n_F chains ("PKE-cluster") rather than independent deformations of single strands.

We have to conclude that stretching of individual strands only cannot explain the macroscopic degree of swelling. Therefore, we investigate the degree of swelling of larger parts of the network structure defined by topological extensions. In Figure 14, the mean square radius of gyration $\langle R_g{}^2(g) \rangle$ of a topological extension of generation g is displayed as a function of its averaged

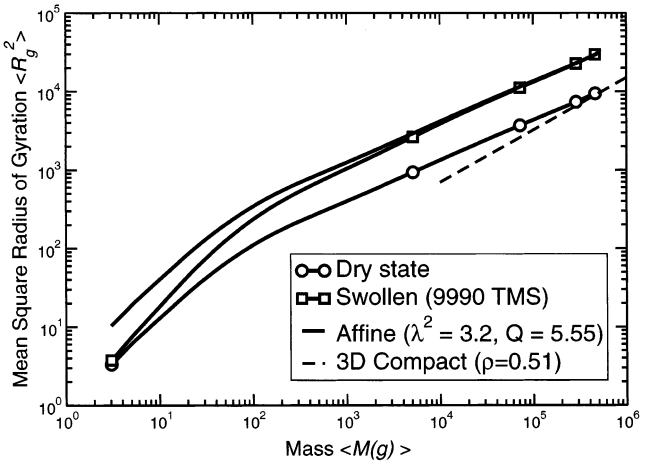

Figure 14. Mean square radius of gyration $\langle R_g^2(g)\rangle$ is plotted vs the mass $M(g)$ calculated successively for each generation g of the topological extension. The results are averaged over all start units for topological extensions selected from a box of size 30 × 30 × 30 in the center of the dry network. The same list of repeat units is used for calculating $\langle R_g(g)\rangle$ in the swollen state. For comparison, the calculated affine behavior is plotted.

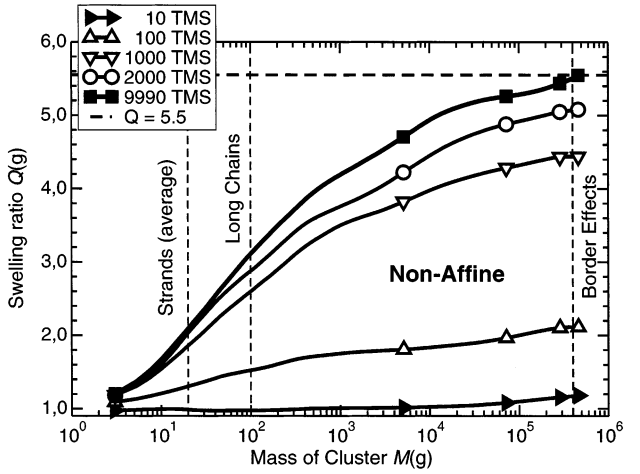

Figure 15. Swelling ratio $Q(g)$ of topological extensions of g generations vs mass of these structures. The size of averaged strands and long strands are indicated.

mass $\langle M(g)\rangle$ (in monomer units) before and after swelling. The data for the dry state correspond to those displayed in Figure 6b. We used exactly the same lists of repeat units to calculate $\langle R_g^2(g)\rangle$ in the swollen state. For comparison, we have displayed the behavior that is expected according to the affine hypothesis.

The crossover effect of the degree of swelling can be better analyzed by calculating the averaged swelling ratio $Q(g)$ as a function of the generation g of topological extensions. The result is plotted in Figure 15 again vs the mass for different times of swelling. Let us consider first the behavior of the network swollen for the longest time (which is close to equilibrium). The macroscopic swelling ratio is only reached for very large structures comprising more than 100 000 repeat units. In the figure, we have indicated the scale of single strands. Apparently there is no impact of the mass of the averaged network strands or even that of the long chains on the crossover behavior of the degree of swelling $Q(M(g))$. Structures containing several 10 000 repeat units still display a marked subaffine behavior. Hence, the missing deformation of individual strands is compensated by unfolding of large structures as proposed in section 2.

A direct visualization for the nonaffinity of the swelling deformation can be obtained in the following way. We virtually cut out a cubic box at the center of the simulation box and follow the displacement of the contained monomers during the swelling process. According to the affine hypothesis, aspect ratio and the form of the cubic box should be conserved on scales larger than the averaged strand length. Note that according to more elaborate network models[5,9] the cross-links are localized and thus fluctuate even less than the average distance of a strand length! To this end, we select all monomers within a box of size 80 × 80 × 80 of the dry network. The box contains 804 cross-links, and its linear extension thus corresponds to about eight strands on average. Now, we consider the conformation of these monomers after swelling. In Figure 16, we have overlayed both pictures before and after swelling taking the cross-links only (There are about 64 000 monomers within the selected sub-box.). The positions after swelling are displayed as bright and opaque spheres, while positions in the dry state are represented as dark, solid spheres. The monomers forming a cubic box in the "folded" state unfold into an almost shapeless structure during swelling. Some of the cross-links moved over very large distances. This process is very much similar to the everyday experience of unfolding of a sheet of paper which has been crumpled up into a paper ball.

Conclusions

We have investigated the internal structure and the swelling behavior of bimodal networks for large ratio of both chain lengths $N/P \gg 1$. A particular interesting situation occurs when the short chains form the minority concerning the volume fraction (monomer fraction) but provide the majority concerning the mole fraction (chain end fraction). Here, during cross-linking clusters of short chains are formed due to the induced composition instability. Resulting from a high nonequilibrium situation, the statistical properties of these clusters will be governed by the cross-linking kinetics. As an estimate for the crossover from homogeneous to a clustered, heterogeneous structure we have derived the inequality $N \gg P^{3/2}$. In our simulation, the onset of short chain clustering is observed, although the short chains are not far away from their overlap threshold. Next, we have analyzed the topological properties by considering topological connected parts of the network (topological extension of a given monomer). From this "internal point of view", the network can be characterized as a folded structure. The distribution of folding lengths shows a broad maximum for large values of paths connecting to neighboring monomers in space.

Very long simulation runs have been carried out to follow the local deformation processes of the network structure during isotropic and athermal swelling. We found that close to swelling equilibrium the deformation of individual strands is much lower (subaffine) than the external deformation. Even the long chains still display subaffine behavior. By considering large clusters of connected monomers, we found profound subaffine deformation even in the range of several 10 000 monomers. Only if the substructures reach a size of much more than 100 000 monomers (thus forming an substantial part of the whole system) is affine behavior

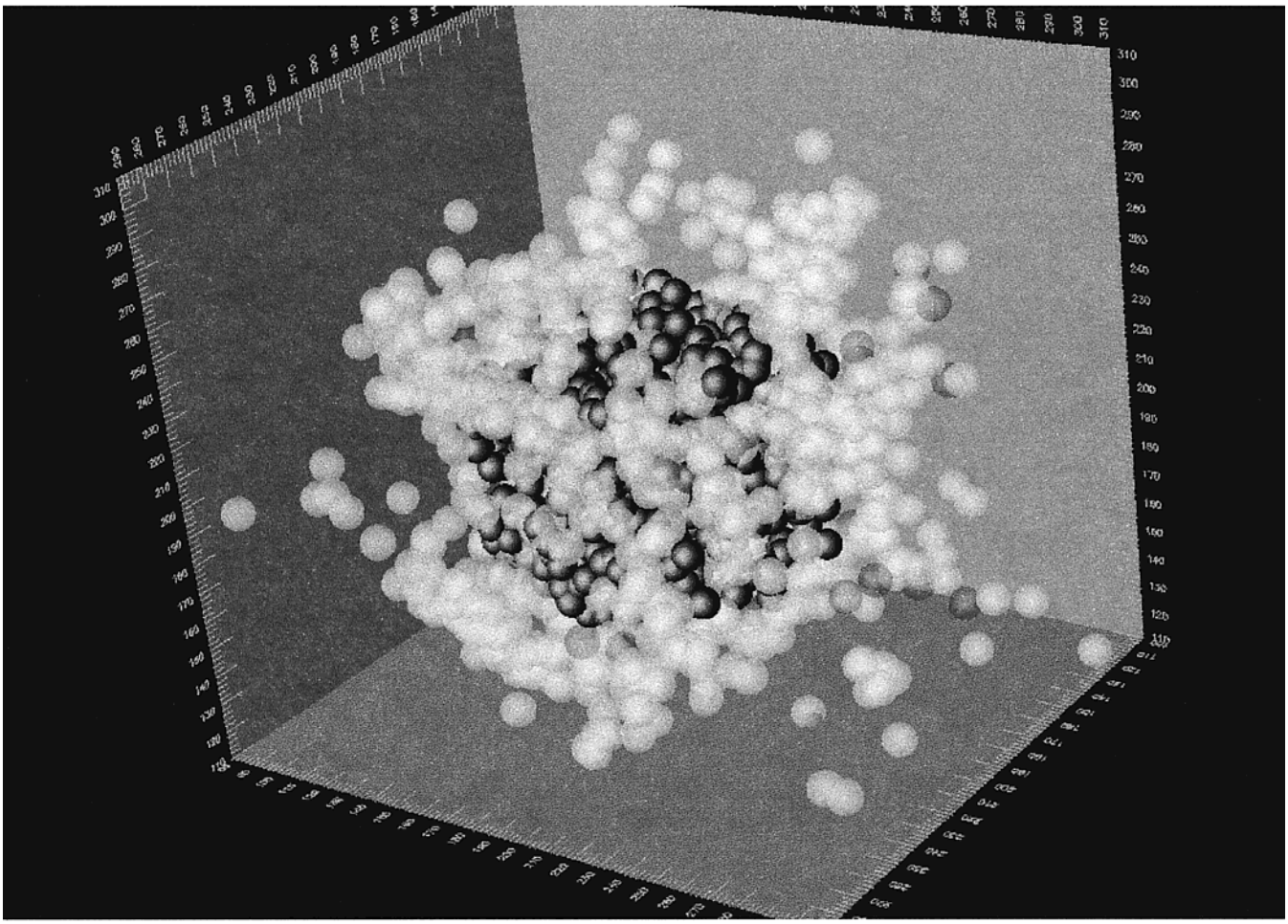

Figure 16. Snapshot of the conformations of cross-links obtained from a cubic part at the center of the dry network (80 × 80 × 80 lattice cites). Only cross-links from the gel fraction are considered. A snapshot of the position of the cross-links is taken before and after swelling. The position after swelling are displayed bright and opaque and are directly superposed to the positions of the cross-links before swelling. Only cross-links outside the original volume are visible for the swollen conformation.

recovered. These quantitative results can be illustrated by direct visualization of swelling of connected clusters and large, geometrically regular parts of the network.

We note that *very long simulation times are absolutely indispensable to obtain reliable results*. In particular in the dry state, conformations can be trapped in a metastable way in parts of the conformational phase space, similarly to what is expected in other disordered systems.[49,50] Such a behavior could than mimic the localization of cross-links as it is assumed in theoretical models. In our simulations we needed about 8 000 000 Monte Carlo steps to equilibrate the swollen system at a lattice density of about 0.1. While a large part of the volume swelling takes place on the time scale comparable to a few Rouse periods of the long chains, the dynamical processes which lead to true swelling equilibrium take place on a time scale which corresponds to thousands of Rouse times of network strands of average length (or some tens of Rouse-relaxation times of long chains). To test the localization of cross-links in the dry state, even longer simulation runs are underway for both bimodal and monomodal end-linked networks.

Acknowledgment. Discussions with O. Spyckerelle, A. Vidal, and B. Haidar are gratefully acknowledged.

References and Notes

(1) James, H. M. *J. Chem. Phys.* **1947**, *15*, 651−668.
(2) Eichinger, B.; Martin, J. *J. Chem. Phys.* **1978**, *69*, 4595−4599.
(3) Shy, L.; Eichinger, B. *J. Chem. Phys.* **1989**, *90*, 5179−5189.
(4) Sommer, J.-U.; Schulz, M.; Trautenberg, H. *J. Chem. Phys.* **1993**, *98*, 7515−7520.
(5) Flory, P. J. *Proc. R. Soc. London* **1976**, *351A*, 351−380.
(6) Soni, V.; Stein, R. S. *Macromolecules* **1990**, *23*, 5257−5265.
(7) Bastide, J.; Picot, C. *J. Macromol. Sci.—Phys.* **1981**, *19*, 13−34.
(8) Bastide, J.; Leibler, L.; Prost, J. *Macromolecules* **1990**, *23*, 1821−1825.
(9) Deam, R. T.; Edwards, S. F. *Philos. Trans. R. Soc. London A* **1976**, *280*, 317−353.
(10) Heinrich, G.; Straube, E.; Helmis, G. *Adv. Polym. Sci.* **1988**, *85*, 34.
(11) Panyukov, S.; Rabin, Y. *Phys. Rep.* **1996**, *269*, 1−131.
(12) Duering, E. R.; Kremer, K.; Grest, G. S. *Phys. Rev. Lett.* **1991**, *67*, 3531−3534.
(13) Trautenberg, H. L.; Sommer, J.-U.; Göritz, D. *J. Chem. Soc., Faraday Trans.* **1995**, *91*, 2649−2653.
(14) Everaers, R.; Kremer, K. *Macromolecules* **1995**, *28*, 7291−7294.
(15) Sommer, J.-U.; Vilgis, T. A.; Heinrich, G. *J. Chem. Phys.* **1994**, *100*, 9181−9191.
(16) Everaers, R.; Kremer, K. *Phys. Rev. E* **1996**, *53*, R37−R40.
(17) Escobedo, F. A.; de Pablo, J. J. *J. Chem. Phys.* **1996**, *104*, 4788.
(18) Escobedo, F. A.; de Pablo, J. J. *J. Chem. Phys.* **1997**, *106*, 793.
(19) Everaers, R. *New J. Phys.* **1999**, *1*, 12.
(20) Sommer, J.-U. *Macromol. Symp.* **1994**, *81*, 139.
(21) Lay, S.; Sommer, J.-U.; Blumen, A. *J. Chem. Phys.* **1999**, *110*, 12173−12182.
(22) Lay, S.; Sommer, J.-U.; Blumen, A. *J. Chem. Phys.* **2000**, *113*, 11355−11363.
(23) Hirokawa, Y.; Jinnai, H.; Nishikawa, Y.; Okamoto, T.; Hashimoto, T. *Macromolecules* **1999**, *32*, 7093−7099.

(24) Plazek, D. J. *J. Polym. Sci. A* **1966**, *4*, 745−763.
(25) Sperling, L. H. *J. Polym. Sci. A* **1968**, *6*, 259.
(26) Chasset, R.; Thirion, P. *Proceedings of the Conference on Physics of Noncristalline Solids*; North-Holland Publ., & Co.: Amsterdam, 1965.
(27) Ferry, J. D. *Viscoelastic Properties of Polymers*, 2nd ed.; John Wiley & Sons Inc.: New York, 1970.
(28) Havranek, A. *Rheol. Acta (Suppl.)* **1988**, *26*, 202−204.
(29) Sommer, J.-U. Beiträge zur Langzeitdynamik von Polymeren Netzwerken. Ph.D. Thesis, TH Merseburg, Merseburg, Germany, 1991.
(30) Sommer, J.-U. *Prog. Colloid Polym. Sci.* **1992**, *90*, 43−46.
(31) Sommer, J.-U. *J. Chem. Phys.* **1991**, *95*, 1316.
(32) Sommer, J.-U.; Russ, T.; Brenn, R.; Geoghegan, M. *Europhys. Lett.* **2002**, *57*, 32−38.
(33) Kuhn, W. *Kolloidzeitschrift* **1936**, *76*, 258−271.
(34) Wall, F. T. *J. Chem. Phys.* **1942**, *10*, 485−488.
(35) Gaylord, R. J.; Douglas, J. F. *Polym. Bull. (Berlin)* **1987**, *18*, 347.
(36) Sommer, J.-U. *J. Chem. Phys.* **1992**, *97*, 5777.
(37) Carmesin, I.; Kremer, K. *Macromolecules* **1988**, *21*, 2819−2823.
(38) Paul, W.; Binder, K.; Kremer, K.; Heermann, D. W. *Macromolecules* **1991**, *24*, 6332−6334.
(39) Mark, J. E. *Elastomers and Rubber Elasticity*; ACS Symposium Series 193; American Chemical Society: Washington, DC, 1982.
(40) li Wu, W.; Coyne, L. D.; Jong, L.; Hanyu, A.; Stein, R. S. *Macromolecules* **1990**, *23*, 351−353.
(41) de Gennes, P. G. *Scaling Concepts in Polymer Physics*; Cornell University Press: Ithaca, NY, 1979.
(42) Raphael, E.; Gay, C.; deGennes, P. G. *J. Stat. Phys.*. **1997**, *89*, 111−118.
(43) Smith, T.; Haidar, B.; Hedrick, J. *Rubber Chem. Technol.* **1990**, *63*, 256.
(44) Flory, P. J.; Rehner, J. *J. Chem. Phys.* **1943**, *11*, 521−526.
(45) Gee, G.; Herbert, J. B. M.; Roberts, R. C. *Polymer* **1965**, *6*, 541.
(46) Gottlieb, M.; Gaylord, R. J. *Macromolecules* **1984**, *17*, 2024.
(47) Oikawa, H.; Murakami, K. *Macromolecules* **1991**, *24*, 1117−1122.
(48) Pütz, M.; Kremer, K.; Everaers, R. *Phys. Rev. Lett.* **2000**, *84*, 298−301.
(49) Goldbart, P.; Goldenfeld, N. *Phys. Rev. A* **1989**, *39*, 1402−1411.
(50) Goldbart, P.; Goldenfeld, N. *Phys. Rev. A* **1989**, *39*, 1412−1419.

MA0205515